Forschungszentrum Karlsruhe

in der Helmholtz-Gemeinschaft

Wissenschaftliche Berichte

FZKA 6702

Magnetohydrodynamic flow in ferromagnetic pipes

L. Bühler

Institut für Kern- und Energietechnik
Programm Kernfusion

Forschungszentrum Karlsruhe GmbH, Karlsruhe
2002

Impressum der Print-Ausgabe:

Als Manuskript gedruckt

Forschungszentrum Karlsruhe GmbH
Postfach 3640, 76021 Karlsruhe

Mitglied der Hermann von Helmholtz-Gemeinschaft
Deutscher Forschungszentren (HGF)

ISSN 0947-8620

Magnetohydrodynamic flow in ferromagnetic pipes

Abstract

The major part of the magnetohydrodynamic pressure drop in the European water cooled concept for a fusion blanket arises in the circular pipes which distribute the liquid metal breeder among the poloidal containers. These channels are surrounded by a very massive structure of electrically conducting ferromagnetic material. The present work highlights the key problems which concern pressure drop and flow distribution in circular pipes with thick conducting walls. The point which has not been investigated in the past is the influence of ferromagnetic wall material. The wall acts like a magnetic shielding for moderate external magnetic fields. The field inside the pipe is strongly reduced and as a result also the magnetohydrodynamic pressure drop. For conditions relevant for applications in fusion blankets the magnetic shielding is not as perfect since the wall material reaches magnetic saturation at the very strong external fields required for the magnetic confinement of the fusion plasma. Therefore the reduction of pressure drop is small for magnetic fields which are much larger than the saturation field of the wall material. The most interesting regime exists near the magnetic saturation where curvilinear field lines inside the pipe are observed. They result in velocity profiles which differ from the well known classical solutions.

Magnetohydrodynamische Strömungen in ferromagnetischen Rohren

Zusammenfassung

Der Hauptanteil der magnetohydrodynamischen Druckverluste im Europäischen wassergekühlten Fusionsblanket entsteht in kreisförmigen Rohren, die den Flüssigmetall-Brutstoff auf die poloidalen Container verteilen. Diese Kanäle sind von massiven, elektrisch leitenden, ferromagnetischen Strukturen umgeben. Die wichtigen Fragen bezüglich Druckverlust und Strömungsverteilung in dickwandigen, elektrisch leitenden Rohren werden in diesem Bericht beantwortet. Ein Punkt, der bisher nicht beachtet wurde, ist der Einfluss ferromagnetischer Wände. Für moderate Magnetfelder wirkt eine solche Wand als magnetische Abschirmung. Das Magnetfeld im Rohr sowie der magnetohydrodynamische Druckverlust werden stark reduziert. Für fusionsrelevante Bedingungen ist die Abschirmung nicht mehr so perfekt, da das Wandmaterial bei den hohen Feldstärken, die zum Plasmaeinschluss benötigt werden, die magnetische Sättigung erreicht. Aus diesem Grund ist die Reduktion des Druckverlusts für Magnetfelder, die stärker sind als die Sättigungsfeldstärke des Wandmaterials, klein. In der Nähe der Sättigungsfeldstärke findet man im Inneren des Kanals gekrümmte magnetische Feldlinien. Diese führen zu Geschwindigkeitsverteilungen, die von den bekannten klassischen Lösungen abweichen.

Magnetohydrodynamic flow in ferromagnetic pipes

Contents

1 Introduction

The knowledge about the magnetohydrodynamic (MHD) pressure drop and the flow structure in pipes made of ferromagnetic material with thick walls is of importance for the European water cooled concept of a fusion blanket. The header of this blanket will be fabricated from ferromagnetic MANET steel which has according to Ruatto (1996) relative magnetic permeabilities up to $\mu_w = 400$. On the other hand the saturation magnetization is considerably large with $M_s \approx 1.65\,\mathrm{T}$, which is of similar order of magnitude than the externally applied magnetic field $B_0 = 6 - 8\,\mathrm{T}$ required for plasma confinement. The pressure drop in most of the blanket is reactively small except in the headers where the flow of the liquid-metal breeder is distributed to and collected from the poloidal containers. A sketch of the blanket with the headers is shown in Fig. 1.

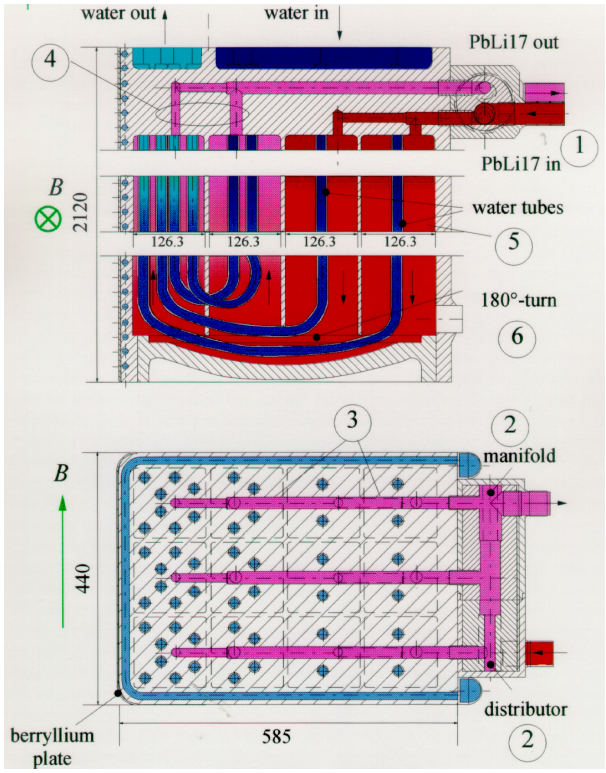

Figure 1: Sketch of the European water-cooled liquid-metal blanket

Flows in circular pipes have been the subject of a number of studies since the early 60th of the last century. Pressure drop and flow pattern are known for a variety of applications. If the magnetic field is very strong Shercliff (1953) derived a solution by asymptotic techniques for walls which are electrically insulating. An exact solution has been published by Gold (1962). Asymptotic solutions for conducting thin walls have been given by Shercliff (1956) and Shercliff (1962) or by Chang and Lundgren (1961). All analyses assumed that the walls confining the electrically conducting fluid are made of non-ferromagnetic material, i.e. the transverse component of the magnetic field inside the pipe is the same as outside and therefore known.

The wall material in the European water-cooled blanket now has ferromagnetic properties so that care has to be taken when the results mentioned above are applied. For relatively small applied external fields $B_0 \ll M_s$, where M_s stands for the saturation of magnetization the wall acts like a magnetic shield and reduces the field inside the pipe to very small values. On the other hand, for $B_0 \gg M_s$ the wall material reaches its magnetic saturation and the field inside the pipe is close to the external field B_0. Between both liner limits there exists a strongly nonlinear regime in which the relative permeability depends essentially on the magnitude of the magnetic field itself. Solutions in this regime are unknown to the knowledge of the author and subject of the present study.

2 Formulation

2.1 Governing equations

The magnetohydrodynamic flow of a conducting viscous incompressible fluid though a pipe is governed by the momentum equation

$$\rho\left[\partial_t \mathbf{v} + (\mathbf{v}\cdot\nabla)\,\mathbf{v}\right] = -\nabla p + \rho\nu\nabla^2\mathbf{v} + \mathbf{j}\times\mathbf{B} \tag{1}$$

with

$$\nabla\cdot\mathbf{v} = 0, \tag{2}$$

where $\mathbf{v}$ is the fluid velocity and p stands for the pressure. The Lorentz force $\mathbf{j}\times\mathbf{B}$ determines the interaction of the electric currents $\mathbf{j}$ with the vector field of magnetic induction $\mathbf{B}$. For simplicity we call $\mathbf{B}$ the magnetic field throughout this manuscript. The fluid has a density ρ and a kinematic viscosity ν.

The currents and the magnetic field are related to each other via Ampère's law

$$\nabla\times\frac{1}{\mu}\mathbf{B} = \mathbf{j}, \tag{3}$$

with the consequence that the currents are solenoidal, i.e.

$$\nabla\cdot\mathbf{j} = 0. \tag{4}$$

Ohm's law gives the coupling with the velocity field due to the induced electric field $\mathbf{v}\times\mathbf{B}$ caused by by the fluid motion.

$$\mathbf{j} = \sigma\left(\mathbf{E} + \mathbf{v}\times\mathbf{B}\right) \tag{5}$$

In these equations μ and σ are the permeability and conductivity of the material and $\mathbf{E}$ stands for the electric field. The electric and magnetic fields are coupled via Faraday's law

$$\nabla\times\mathbf{E} = -\partial_t\mathbf{B} \tag{6}$$

requiring a solenoidal magnetic field

$$\nabla\cdot\mathbf{B} = 0. \tag{7}$$

The latter condition is satisfied identically by introducing a vector potential $\mathbf{A}$ such that

$$\mathbf{B} = \nabla\times\mathbf{A}. \tag{8}$$

With this definition Faraday's law becomes

$$\mathbf{E} = -\nabla\phi - \partial_t\mathbf{A}, \tag{9}$$

where the electric field is determined by the gradient of the scalar electric potential ϕ and the temporal changes in the magnetic vector potential $\mathbf{A}$.

In the following we substitute $\mathbf{B}$ in (3) by its vector potential (8) and introduce the result in (5). This yields

$$\nabla \times \left(\frac{1}{\mu} \nabla \times \mathbf{A} \right) = \sigma \left(-\nabla \phi - \partial_t \mathbf{A} + \mathbf{v} \times \nabla \times \mathbf{A} \right). \tag{10}$$

The equations shown above apply in the fluid as well as in the wall or outside the wall. Note, the wall generally has a conductivity and permeability different from those of the fluid and the exterior domain is usually the non-conducting atmosphere.

2.2 Nondimensional equations

We multiply the equation (10) with the permeability of free space μ_0 and find with the characteristic scales v_0, L, B_0, $B_0 L$, and $v_0 B_0 L$ for velocity, length, magnetic field, magnetic potential, and electric potential the nondimensional form for stationary problems

$$\nabla \times \left(\frac{1}{\mu_r} \nabla \times \mathbf{A} \right) = R_m \sigma_r \left(-\nabla \phi + \mathbf{v} \times \nabla \times \mathbf{A} \right), \tag{11}$$

where μ_r and σ_r stand for the relative permeability and conductivity of the materials, respectively compared with the non-ferritic fluid. The values for μ_r depend on the material and range from 1 for non-ferritic materials as the fluid to 10^3 for ferritic steel. In applications considered in the following the fluid domain is bounded by a wall that consists of a single material so that we have $\mu_r = \sigma_r = 1$ in the fluid and $\mu_r = 1$ and $\sigma_r = 0$ in the insulating atmosphere surrounding the pipe. For the wall we generally have different values and denote them as $\mu_r = \mu_w$ and $\sigma_r = \sigma_w$. The magnetic Reynolds number

$$R_m = \sigma \mu_0 v_0 L \tag{12}$$

gives the ratio of the magnetic field induced by the flow and the externally applied field. R_m is small in laboratory or engineering applications with typical values on the order of $R_m < 10^{-2}$.

Introducing nondimensional notation in the momentum equation yields

$$N^{-1} \left[\partial_t \mathbf{v} + (\mathbf{v} \cdot \nabla) \mathbf{v} \right] = -\nabla p + Ha^{-2} \nabla^2 \mathbf{v} + \mathbf{j} \times \mathbf{B}, \tag{13}$$

where now p represents the pressure scaled by $\sigma v_0 B_0^2 L$. The nondimensional groups

$$N = \frac{\sigma L B_0^2}{\rho v_0} \tag{14}$$

and

$$Ha = L B_0 \sqrt{\frac{\sigma}{\rho \nu}} \tag{15}$$

are the interaction parameter and Hartmann number, which account for the importance of electromagnetic forces compared with inertia and viscous friction, respectively. For applications to fusion relevant flows $N = 10^2 - 10^4$ and $Ha = 10^3 - 10^4$.

3 Analysis

3.1 The magnetic field

The smallness of R_m suggests to expand the magnetic potential in a power series as

$$\mathbf{A} = \mathbf{A}_0 + R_m \mathbf{A}_1 + O\left(R_m^2\right). \tag{16}$$

This yields at leading order

$$\nabla \times \left(\frac{1}{\mu_r} \nabla \times \mathbf{A}_0\right) = 0. \tag{17}$$

The leading order magnetic field is unaffected by the flow. If we restrict the analysis to the case of a transverse magnetic field with $\mathbf{B} \cdot \hat{\mathbf{x}} = 0$, uniform along the axis, the magnetic potential has only a single component as $\mathbf{A}_0 = A(y,z)\,\hat{\mathbf{x}}$. If other nonuniform components of $\mathbf{A}_0$ were present the magnetic field would vary along the axis and the assumption of a fully established flow would no longer be justified. These assumptions reduce (17) to

$$\nabla \cdot \left(\frac{1}{\mu_r} \nabla A\right) = 0, \tag{18}$$

Therefore we have to solve a scalar equation of heat conduction type where $\mu_r = 1$ in the fluid and in the insulating surrounding atmosphere and $\mu_r = \mu_w$ in the wall. At large distance from the duct wall the magnetic field is unperturbed by the presence of the pipe with a single component in the y-direction, $\mathbf{B} = \hat{\mathbf{y}}$. This requires for the magnetic potential that

$$\partial_z A = 1,\ \partial_y A = 0 \quad \text{as} \quad y, z \to \infty. \tag{19}$$

For geometry and coordinates see Fig. 2.

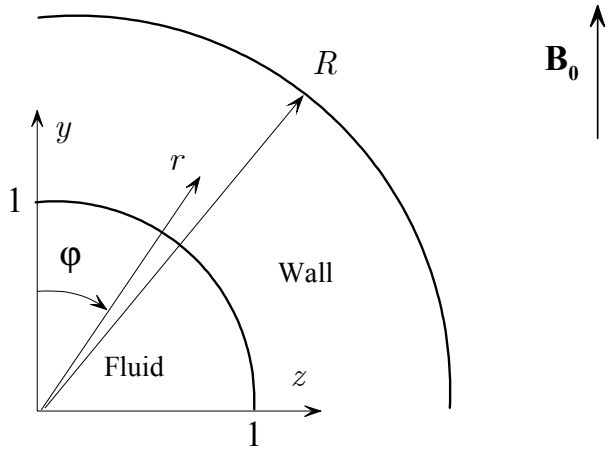

Figure 2: Sketch of geometry and coordinates

The equation (18) with the condition (19) determines the problem uniquely. For practical reasons we split the computational domain into three subregions. One is the

wall region where we solve the nonlinear equation

$$\nabla \cdot \left(\frac{1}{\mu_w} \nabla A \right) = 0. \tag{20}$$

The function $\mu_w(\nabla A)$ is determined by the magnetization properties of the material. The other subregions are the interior and exterior regions where the linear equation

$$\nabla \cdot (\nabla A) = 0 \tag{21}$$

can be satisfied much easier by either analytical solutions or via boundary integral methods. The conditions at interfaces between different materials become

$$\left[\frac{1}{\mu_r} \partial_n A \right] = 0, \tag{22}$$

$$[A] = 0, \tag{23}$$

where [ ] denotes the jump across the interface. For general solutions we apply an iterative numerical scheme which solves for the iteration step the nonlinear equation (20) by efficient numerical techniques for given Dirichlet conditions at the interior and exterior surface of the wall. The calculated approximation for A in the wall determines via (22) the normal derivatives $\partial_n A$ outside and inside the pipe and, as a matter of fact, the global solutions for A. Once improved estimates for A in the pipe and in the exterior region are found we impose the values according to (23) on the wall surfaces as Dirichlet conditions for the next iteration.

3.2 Magnetization of the wall material

For applications in fusion engineering the magnetic field confining the plasma is so strong that the wall material reaches its magnetic saturation. A typical hysteretic magnetization behavior is shown in Fig. 3. We follow the suggestions of Ruatto (1996) and neglect for the moment the magnetic hysteresis. For first calculations we propose an approximation of the magnetization curve by two linear parts as shown in the figure with

$$B = \begin{cases} \mu_{w,l} B_0 & \text{ferritic} \\ M_s + B_0 & \text{saturated} \end{cases}. \tag{24}$$

where $B_0 = \mu_0 H$. The quantity $\mu_{w,l}$ is the relative permeability in the linear ferritic regime and M_s characterizes the magnetic saturation. The approximation has the advantage that the function $B(B_0)$ can be simply inverted. This equation ensures a linear non-ferritic behavior as the externally applied magnetic field is very large, i.e.

$$B \to B_0 \quad \text{as } B_0 \to \infty, \tag{25}$$

but exhibits ferritic character for small magnetic fields, for which we use a linear approximation for the ferritic regime with permeability $\mu_{w,l}$. The global behavior is determined once the magnetic saturation M_s and $\mu_{w,l}$ are known.

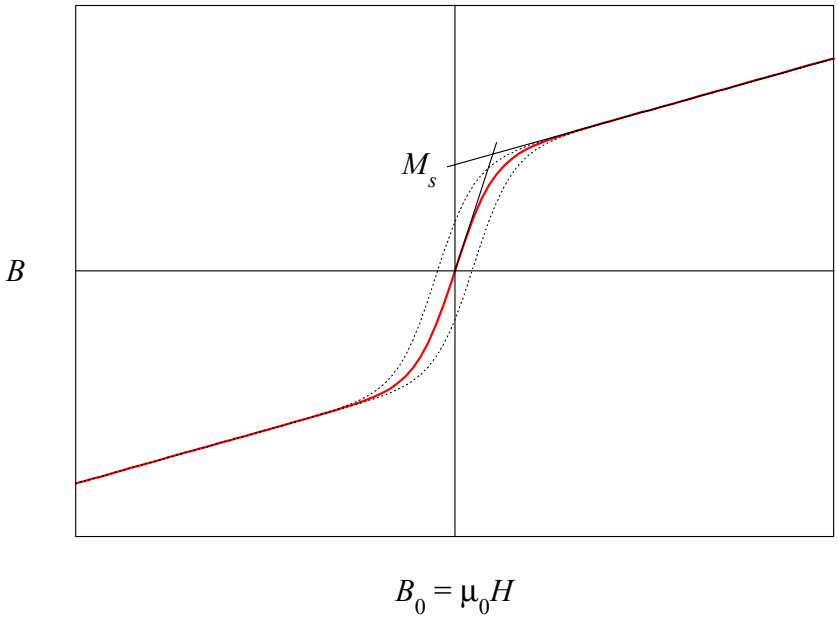

Figure 3: Typical magnetization behavior of ferromagnetic materials.

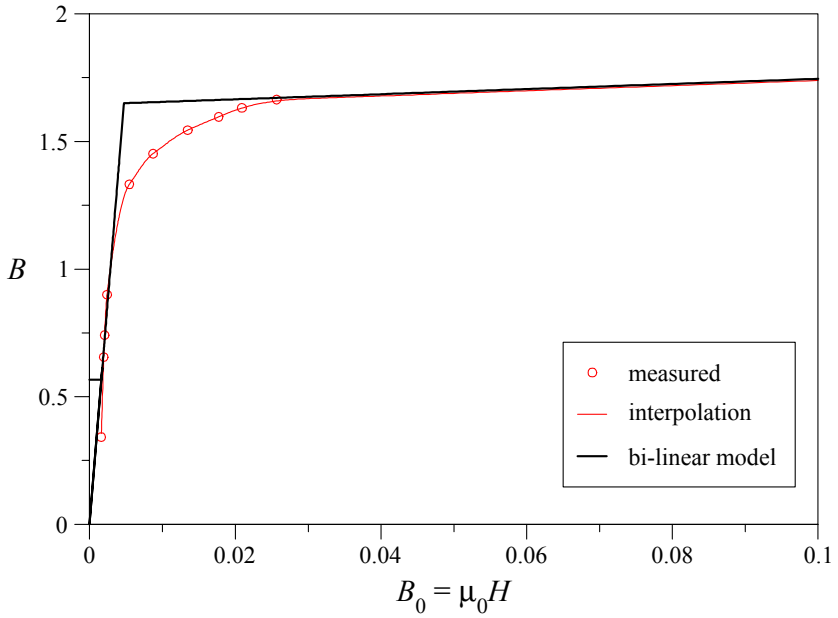

Figure 4: Measured magnetization of MANET and model proposed for numerical calculations

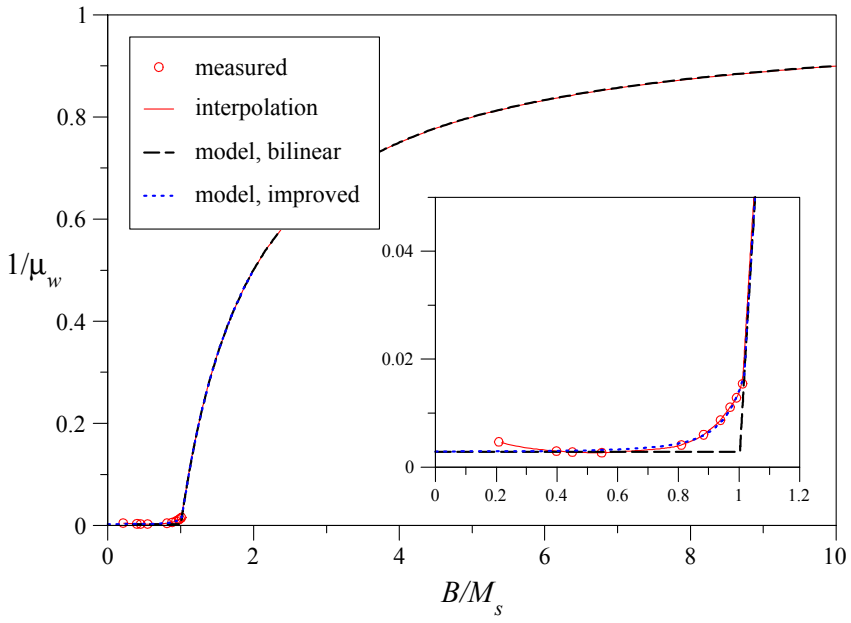

Figure 5: Dependence of $1/\mu_w$ as a function of B/M_s for MANET. Comparison of model and measured data

For numerical calculations it is important to know the value of $\mu_w = B/B_0$ or

$$\frac{1}{\mu_w} = \frac{B_0}{B} = \begin{cases} \mu_{w,l}^{-1} & \text{ferritic} \\ 1 - \frac{M_s}{B} & \text{saturated} \end{cases} . \tag{26}$$

The quantity μ_w^{-1} approaches unity as $B \gg M_s$ in the saturated regime but exhibits ferritic behavior with $\mu_w = \mu_{w,l}$ as $B \leq M_s$. The variation of μ_w^{-1} with the strength of the applied magnetic field is shown in Fig. 5. Ruatto (1996) determined the magnetic permeability (or the susceptibility) from measured data for the ferritic MANET steel which is foreseen as structural material for fusion blankets. If we replot his data we find a situation as shown in Fig. 4 or in Fig. 5. As B approaches M_s the measured quantity μ_w^{-1} deviates from the bilinear model. We therefore use a modified relation such as

$$\frac{1}{\mu_w} = \frac{B_0}{B} = \begin{cases} \mu_{w,l}^{-1} \left(1 + \left(\frac{0.43}{B/M_s - 1.305} \right)^4 \right) & \text{ferritic} \\ 1 - \frac{M_s}{B} & \text{saturated} \end{cases} , \tag{27}$$

which approximates the real situation much better.

3.3 The flow

Solutions of the equations displayed above for the magnetic field will show that in general the magnetic field inside a duct may vary in the transverse direction and that the field lines are possibly curved. Therefore, classical solutions known for MHD pipe flows do not cover all applications under consideration. In the following subsection we assume that the magnetic field is known inside the fluid region. We derive an asymptotic solution for fully developed flows that is valid for strong, non-uniform magnetic fields.

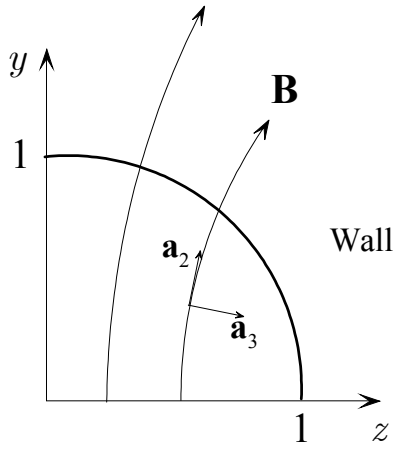

Figure 6: Magnetic coordinates

For fully developed stationary conditions the velocity and pressure gradient have only a single component along the axis $\mathbf{v} = U\,\hat{\mathbf{x}}$, $\nabla p = -k\hat{\mathbf{x}}$, while electric currents flow in the plane of the cross section as $\mathbf{j}\cdot\hat{\mathbf{x}} = 0$. For high Hartmann numbers viscous effects are confined to thin boundary layers along the duct wall while most of the flow is carried by the inviscid core. Boundary layers in which the magnetic field has a significant normal component are called the Hartmann layers.

3.3.1 Magnetic coordinates

Formulations of MHD problems for arbitrary magnetic fields have been given by Kulikovskii (1974), Bühler (1995) or by Alboussière, Garandet and Moreau (1996). Here we use a curvilinear orthogonal coordinate system defined by the base vectors

$$\begin{aligned} \mathbf{a}_1 &= \hat{\mathbf{x}}, \\ \mathbf{a}_2 &= \nabla A \times \hat{\mathbf{x}} \quad (= \mathbf{B}), \\ \mathbf{a}_3 &= \tfrac{1}{(\nabla A)^2}\nabla A. \end{aligned} \tag{28}$$

In this coordinate system the vector $\mathbf{a}_2$ coincides with the magnetic field since we had $\mathbf{B} = \nabla \times (A\hat{\mathbf{x}}) = \nabla A \times \hat{\mathbf{x}} = \mathbf{a}_2$. The axial direction, now denoted by $\mathbf{a}_1$, remains unchanged and $\mathbf{a}_3$ is the transverse direction, orthogonal to both, the axis of the pipe and the magnetic field. For details see Fig. 6 The metric tensor $g_{ik} = \mathbf{a}_i \cdot \mathbf{a}_k$ has only diagonal entries and reads as

$$g_{ik} = \begin{bmatrix} 1 & 0 & 0 \\ 0 & B^2 & 0 \\ 0 & 0 & B^{-2} \end{bmatrix}, \tag{29}$$

with $B^2 = (\nabla A)^2$. Any vector quantify $\mathbf{f}$ may be expressed by contravariant components f^i as $\mathbf{f} = f^i\mathbf{a}_i$ of the general base but also by covariant components as $\mathbf{f} = f_k\mathbf{a}^k$ of the reciprocal base for which $\mathbf{a}_i \cdot \mathbf{a}^k = \delta_i^k$. Co- and contravariant vector components are

related to each other by the metric coefficients as $f_i = g_{ik} f^k$. A line element $d\mathbf{x}$ finds the representation in the new coordinates u^i as

$$d\mathbf{x} = \mathbf{a}_i du^i \tag{30}$$

and a volume element is determined by

$$dV = \sqrt{g} du^1 du^2 du^3 = du^1 du^2 du^3, \tag{31}$$

where g denotes the determinant of the matrix formed by the metric coefficients which evaluates identically to unity. Note, the coordinate u^3 is simply related to the magnetic potential as $u^3 = A$.

3.3.2 The core flow

For fully developed stationary conditions the core velocity and pressure gradient have only a single component along the axis $\mathbf{v}_c = u\,\mathbf{a}_1$, $\nabla p = -k\,\mathbf{a}^1$, while electric currents flow in the plane of the cross section as $\mathbf{j}_c = j^2\mathbf{a}_2 + j^3\mathbf{a}_3$. The inviscid flow in the core is governed by a balance between Lorentz forces and pressure forces as

$$\partial_1 p = -k = -j^3. \tag{32}$$

The current component perpendicular to the field is therefore uniquely determined. Conservation of charge requires a solenoidal current field

$$\partial_i j^i = 0. \tag{33}$$

Ohm's law reads

$$j_2 = -\partial_2 \phi, \tag{34}$$

$$j_3 = -\partial_3 \phi + u. \tag{35}$$

After substituting j^3 according to (32) in (33) we find with the symmetry condition $j^2 = 0$ at $u^2 = 0$ that

$$j^2 = j_2 = 0. \tag{36}$$

Therefore the current density in the core finds the representation as $\mathbf{j}_c = j^3\mathbf{a}_3$. As a consequence Ohm's law yields

$$\partial_2 \phi = 0, \tag{37}$$

which simply states that the electric potential is uniform along magnetic field lines, i.e. magnetic field lines are isolines of potential. Since the potential does not vary along field lines it is sufficient to know the potential at one point along the line, e.g. at the fluid-wall interface. If we suppose for the moment that the core potential at the fluid wall interface is known we may evaluate the core velocity by (35)

$$u = k\left(\frac{1}{B^2} + \frac{\partial \Phi}{\partial A}\right), \tag{38}$$

where we replaced the potential by $\phi = k\Phi$.

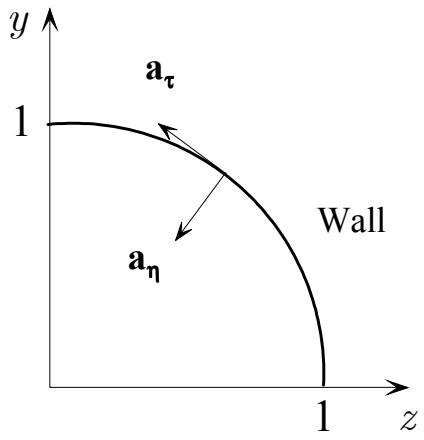

Figure 7: Boundary layer coordinates

3.3.3 Boundary layer coordinates

Knowing that the viscous boundary layers are very thin for strong magnetic fields we stretch the wall normal coordinate by the boundary layer thickness δ and denote it by

$$\eta = \frac{n}{\delta} \text{ with } \delta \ll 1. \tag{39}$$

Here, n is the local coordinate normal to the wall and $\mathbf{n} = \nabla n$ is the the unit normal to the wall at Γ, pointing into the fluid. We further suppose that the magnetic field does not change at leading order across the boundary layer. For the description of the flow in the viscous boundary layers at the duct walls we use a second curvilinear orthogonal coordinate system defined by the base vectors

$$\begin{aligned} \mathbf{a}_1 &= \hat{\mathbf{x}}, \\ \mathbf{a}_\eta &= \delta\, \mathbf{n}, \\ \mathbf{a}_\tau &= \hat{\mathbf{x}} \times \mathbf{n} \quad = \boldsymbol{\tau}. \end{aligned} \tag{40}$$

In this coordinate system the vector $\mathbf{a}_1$ coincides with the channel's axis while $\mathbf{a}_\eta$ points into the fluid, normal to the wall. The third base vector $\mathbf{a}_\tau$ is tangential to the wall. The situation is sketched in Fig. 7. The metric tensor in the layer has only diagonal entries and reads as

$$g_{ik} = \begin{bmatrix} 1 & 0 & 0 \\ 0 & \delta^2 & 0 \\ 0 & 0 & 1 \end{bmatrix}. \tag{41}$$

A line element $d\mathbf{x}$ finds the representation in the new coordinates as

$$d\mathbf{x} = \mathbf{a}_1 du^1 + \mathbf{a}_\eta d\eta + \mathbf{a}_\tau d\tau \tag{42}$$

and a volume element is determined by

$$dV = \sqrt{g} du^1 d\eta\, d\tau = \delta du^1 d\eta\, d\tau. \tag{43}$$

3.3.4 The Hartmann layer flow

We assumed for the flow in the core that viscous effects are negligible and that the flow is balanced by an equilibrium between pressure and Lorentz forces. Viscous effects are confined to thin boundary layers along the walls. We consider now these viscous layers and suppose that a uniquely valid solution in the whole fluid domain is composed by two parts, one is the core solution as derived above and the other is the viscous correction in the boundary layer. As an example we may express the total axial velocity component by U. It is composed by the core velocity and its viscous correction as

$$U = u + u_\delta. \tag{44}$$

The total current density vector may find a representation as

$$\mathbf{j} = j^3 \mathbf{a}_3 + \left(j^\tau \mathbf{a}_\tau + j^\eta \mathbf{a}_\eta\right). \tag{45}$$

For electric potential we can assume a similar relation with ϕ_δ or Φ_δ as viscous corrections. The viscous corrections to the inviscid core solution in the Hartmann layers are needed in order to satisfy no-slip at the walls. The viscous corrections vanish at large distance from the wall, i.e. $(u_\delta,\ j^\tau,\ j^\eta,\ \phi_\delta) \to 0$ as $\eta \to \infty$.

Ohm's law in the boundary layer yields now

$$j_\eta = -\partial_\eta \phi_\delta, \tag{46}$$

$$j_\tau = -\partial_\tau \phi_\delta + \delta\, u_\delta B^\eta, \tag{47}$$

and the momentum equation reduces to

$$\frac{1}{Ha^2}\frac{1}{\delta^2}\partial_{\eta\eta} u_\delta - \delta\, j^\tau B^\eta = 0. \tag{48}$$

The core variables disappear from the boundary layer equations since they satisfy the equations in the inviscid limit. Note, due to the coordinate stretching introduced just above the component of magnetic field $B^\eta = (\mathbf{B}\cdot\mathbf{n})/\delta$ is one order of magnitude larger than $B^\tau{=}(\mathbf{B}\cdot\boldsymbol{\tau})$. For that reason B^τ does not appear in the analysis at this order of approximation. This assumption holds as long as $(\mathbf{B}\cdot\mathbf{n}) \gg (\mathbf{B}\cdot\boldsymbol{\tau})\ \delta$, where $\boldsymbol{\tau}$ stands for a unit vector in the tangential direction. For very thin viscous layers with $\delta \ll 1$ this assumption is fairly valid along most of the pipe wall. It would break down only in a very narrow region near the sides where the magnetic field becomes tangential to the walls. Roberts (1967) pointed out that this region is small for high Hartmann numbers and that it does not affect the core velocity and the pressure drop in the other fluid domain at leading order.

We find in the boundary layer a balance between viscous forces and Lorentz forces. This requires that j^τ is of the same order of magnitude as the viscous forces, say of leading order in the analysis. The conservation of charge

$$\partial_\eta\left(\delta j^\eta\right) + \partial_\tau\left(\delta j^\tau\right) = 0 \tag{49}$$

requires that j^η is of the same order of magnitude. The quantity $j_\eta = g_{\eta\eta} j^\eta = \delta^2 j^\eta$, however, is negligible in Ohm's law for $\delta \ll 1$. Since the viscous correction for potential

disappears at large distance from the wall and since it does not change across the layer according to (46) it is zero in the whole boundary layer, i.e. $\phi_\delta = 0$.

Now we can substitute $j^\tau = j_\tau$ in (48) by (47) and find an ordinary differential equation governing the viscous correction for velocity in the Hartmann layer.

$$\frac{1}{Ha^2 \left(\mathbf{B}\cdot\mathbf{n}\right)^2}\frac{1}{\delta^2}\partial_{\eta\eta}u_\delta - u_\delta = 0. \tag{50}$$

For a reasonable balance of forces we have to keep the viscous term $\partial_{\eta\eta}u_\delta$ in the equation as $Ha \to \infty$ to balance the Lorentz force term $-u_\delta$. This requirement determines the thickness of the viscous layer as

$$\delta = \frac{1}{Ha\left|\mathbf{B}\cdot\mathbf{n}\right|}. \tag{51}$$

The governing equation for velocity reduces to

$$\partial_{\eta\eta}u_\delta - u_\delta = 0 \tag{52}$$

with solution

$$u_\delta = -u_\Gamma \exp\left(-\eta\right). \tag{53}$$

Here, u_Γ is the core velocity taken at the fluid-wall interface Γ. With this correction the velocity vector is entirely determines as

$$\mathbf{v} = \left[u - u_\Gamma \exp\left(-\eta\right)\right]\hat{\mathbf{x}}. \tag{54}$$

It satisfies the no-slip condition at the wall and viscous corrections vanish rapidly with increasing distance to the wall.

After the viscous correction of velocity is obtained we determine $j^\tau = j_\tau$ using (47) as

$$j^\tau = u_\Gamma\left(\mathbf{B}\cdot\mathbf{n}\right)\exp\left(-\eta\right). \tag{55}$$

The viscous correction to the tangential currents in the layer is determined by the velocity of the inviscid core solution and shows exponential decay towards the core. In the next step we substitute these currents into (49) and find

$$\delta\partial_\eta\left(j^\eta\right) + Ha^{-1}\exp\left(-\eta\right)\,\partial_\tau u_\Gamma = 0, \tag{56}$$

an equation that is easily integrable along the wall-normal direction to yield

$$\delta j^\eta\left(\eta = 0\right) - Ha^{-1}\,\partial_\tau u_\Gamma = 0. \tag{57}$$

The quantity $\delta j^\eta\left(\eta = 0\right)$ is the flux of current entering the boundary layer at the interface to the wall. It is determined by the fact that all currents leaving the fluid enter the wall. This requires that

$$\mathbf{j}\cdot\mathbf{n} = j^3\mathbf{a}_3\cdot\mathbf{n} + \delta j^\eta = -\sigma_w\nabla\phi_w\cdot\mathbf{n}. \tag{58}$$

Recalling the definition of the base vector $\mathbf{a}_3$ (28) yields with (32)

$$\frac{1}{B^2}\nabla A\cdot\mathbf{n} + \frac{1}{Ha}\,\partial_\tau\left(\frac{u}{k}\right) = -\sigma_w\nabla\Phi_w\cdot\mathbf{n} \;\text{ at }\Gamma, \tag{59}$$

where we have to take ∇A in the fluid and $\nabla \phi_w$ in the wall. If we further substitute the core velocity at the wall by (38) we find the interface condition for wall potential as

$$\frac{\partial_n A}{B^2} + \frac{1}{Ha}\,\partial_\tau \left(\frac{1}{B^2} + \frac{\partial \Phi}{\partial A} \right) + \sigma_w \partial_n \Phi_w = 0 \ \text{ at } \Gamma. \tag{60}$$

This condition applies to the wall potential at the interface to the fluid while at the interface towards an insulating atmosphere we have $\partial_n \Phi_w = 0$. The equation which determines the potential inside the wall is the Laplace equation

$$\nabla^2 \Phi_w = 0. \tag{61}$$

For applications in engineering the duct wall is either fabricated from metals (steel, copper, etc.) or the wall is insulating (e.g. glass, fiberglass, ceramic materials). In addition, for pressure drop reduction, metallic walls may be covered by an insulating layer to prevent currents induced in the fluid to enter the conducting walls. While the Hartmann number is large for all applications we have in mind the relative conductivity of the walls may be of order unity for metals or negligibility small for insulating walls or for conducting walls which are covered by an insulating layer. In the following we shall discuss these two cases.

If the wall is well conducting, say $\sigma_w \gg Ha^{-1}$, equation (60) finds a major balance between the first and the third term. The physical reason for this balance is that the currents cross the viscous layer unchanged before they enter the conducting wall. They close their circuit inside the wall thus bypassing the viscous layers. The reduced boundary condition for that case reads

$$\frac{\partial_n A}{B^2} + \sigma_w \partial_n \Phi_w = 0 \ \text{ at } \Gamma. \tag{62}$$

We note that the Hartmann number disappears from the analysis. As a matter of fact the solution for the leading order core velocity and for pressure drop becomes independent of the strength of the magnetic field.

The other case of practical interest is that the wall is insulated from the fluid. This happens for $\sigma_w \ll Ha^{-1}$. In the latter case we neglect the currents which enter the wall in comparison with the other terms in (60) and find

$$Ha\, k \frac{\partial_n A}{B^2} + \partial_\tau u = 0 \ \text{ at } \Gamma, \tag{63}$$

an equation that determines directly the core velocity by integration. The first term describes the currents which enter or leave the core from the layer, while u is proportional to the integrated currents in the viscous layer. Now all currents which leave the core enter the viscous layer and change therefore the total current inside the layer along the contour of the pipe. This fixes the constant of integration and the velocity evaluates as

$$u = -Ha\, k \int_0^\tau \frac{\partial_n A}{B^2} d\tau \ \text{at } \Gamma. \tag{64}$$

Note, the tangential coordinate τ has its origin where the magnetic field touches the wall in one point. If we know the velocity at Γ we can extract the quantity $\partial \Phi / \partial A$

which applies to each point along field lines. We substitute the latter quantity in (38) and find the core velocity inside the pipe as

$$u = k\left(\frac{1}{B^2} - \frac{1}{B_\Gamma^2} - Ha\int_0^\tau \frac{\partial_n A}{B^2}d\tau\right). \tag{65}$$

The last two terms on the right-hand side are evaluated at the wall and spread into the fluid along field lines. For planar fields, B and B_Γ are equal so that the first two terms on the right-hand side cancel exactly. If the field lines are curved they generally differ and do not cancel completely. Nevertheless, since $Ha \gg 1$ for all applications we have in mind, the third term is dominant and the core velocity in the whole fluid domain is well approximated as

$$u = -Ha\,k\int_0^\tau \frac{\partial_n A}{B^2}d\tau. \tag{66}$$

This equation is easily evaluated at the fluid-wall interface and, since the velocity does not change along field lines, we know the velocity in the whole fluid region. We note that $\partial_n A = -\mathbf{B}\cdot\boldsymbol{\tau}$ so that the equation determining the core velocity can be expressed also as

$$u = Ha\,k\int_0^\tau \frac{\mathbf{B}\cdot\boldsymbol{\tau}}{B^2}d\tau. \tag{67}$$

Let us apply this condition now to the simple example of a planar magnetic field $\mathbf{B} = \hat{\mathbf{y}}$ for which we find

$$u = Ha\,k\int_0^\tau (\hat{\mathbf{y}}\cdot\boldsymbol{\tau})\,d\tau = Ha\,k\int_o^Y dy = Ha\,kY, \tag{68}$$

where Y denotes the y position of the interface. It is a well known result that for MHD flows in insulating pipes the core velocity profile is proportional to the extension of the duct measured along field lines. This result is very general and applies for ducts on any type of cross section (see e.g. Müller and Bühler (2001)). For circular pipes we have $Y = \cos\varphi$. The flow rate $Q = \int uY dz$ evaluates with $dz = \cos\varphi\, d\varphi$ as

$$Q = Ha\,k\int_0^{\pi/2}\cos^3\varphi d\varphi = \frac{2}{3}Ha\,k. \tag{69}$$

Normalization of the velocity requires that $Q = \pi/4$ which yields the pressure drop as

$$k = \frac{3\pi}{8}\frac{1}{Ha}, \tag{70}$$

is in agreement with results obtained by Shercliff (1962).

4 Circular pipes

In the following we focus on flows in circular pipes which are most widely used in engineering applications. In a first step we restrict the analysis to cases for which the wall material does not reach its magnetic saturation. Cases for which the wall material reaches its magnetic saturation are analyzed in a separate subsection.

4.1 Constant magnetic permeability

We assume that the relative permeability depends only on the material and that it is independent of the magnitude of the applied magnetic field. Such regimes occur for magnetic fields which are much smaller than the saturation field, i.e. $B \ll M_s$. For such cases $\mu_r = 1$ in the fluid and outside the wall. In the wall the permeability $\mu_r = \mu_w$ is constant and can be extracted from the Laplacean. It is further convenient to formulate the problem in cylindrical coordinates

$$x = x, \quad y = r\cos\varphi, \quad z = r\sin\varphi, \tag{71}$$

in which (18) becomes

$$r\partial_r\left(r\partial_r A\right) + \partial_{\varphi\varphi} A = 0. \tag{72}$$

We expand the magnetic potential in a Fourier series such as

$$A = \sum_{i=1}^{\infty} a_i \sin i\varphi \tag{73}$$

and find equations for the Fourier components $a_i(r)$

$$r\partial_r\left(r\partial_r a_i\right) - i^2 a_i = 0. \tag{74}$$

The interface conditions are

$$\left[\frac{1}{\mu_r}\partial_r a_i\right] = [a_i] = 0, \tag{75}$$

and the condition at large distance reads

$$\partial_r a_1 = 1, \quad \partial_r a_i = 0 \text{ for } i > 1. \tag{76}$$

The condition (76) at large distance shows together with (74) that the only nontrivial solution exists for a_1. Applying the interface conditions determines uniquely the solution as

$$a_1 = \begin{cases} \alpha \; r & & & \text{for} & r < 1 \\ \frac{1}{2}\alpha\left(1+\mu_w\right) \; r & + \; \frac{1}{2}\alpha\left(1-\mu_w\right) \; r^{-1} & & \text{for} & 1 < r < R \\ r & + \frac{1}{4}\alpha\left(\mu_w^2 - 1\right)\left(R^2 - 1\right)\mu_w^{-1} \; r^{-1} & & \text{for} & r > r \end{cases} \tag{77}$$

where the coefficient

$$\alpha = 4\frac{\mu_w R^2}{1+\mu_w^2}\left(R + \frac{\mu_w - 1}{\mu_w + 1}\right)^{-1}\left(R - \frac{\mu_w - 1}{\mu_w + 1}\right)^{-1} \tag{78}$$

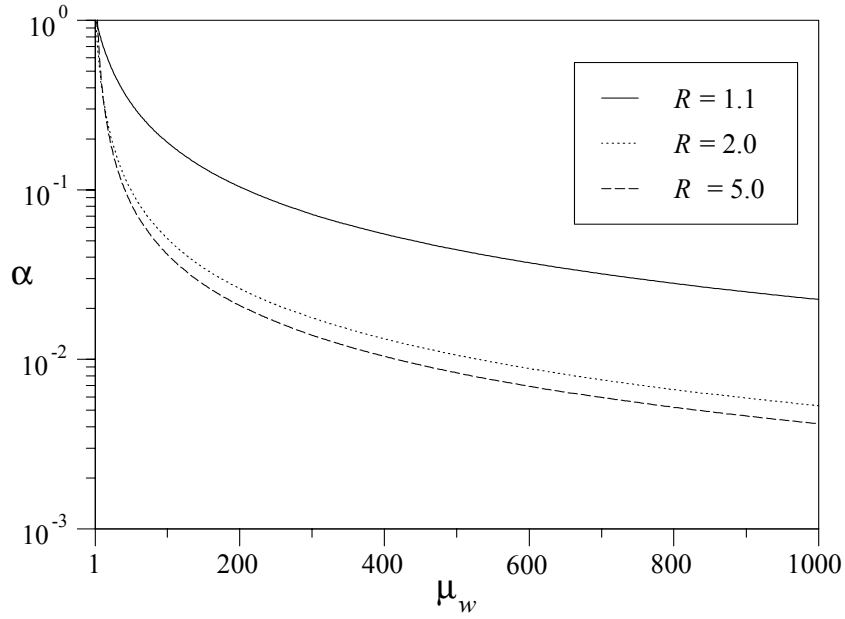

Figure 8: Factor α by which the magnetic field is reduced inside a ferritic circular pipe in comparison with non-ferritic walls. Examples for a thin wall with $R = 1.1$ and for thick walls with $R = 2$ and $R = 5$ are shown

determines the strength of the magnetic field inside the pipe bore hole.

We find that the magnetic potential in the fluid region has the representation as

$$A = \alpha r \sin \varphi = \alpha z. \tag{79}$$

This yields a strength of the magnetic field in the pipe as

$$\mathbf{B} = \nabla \times (A\hat{\mathbf{x}}) = \alpha \hat{\mathbf{y}}. \tag{80}$$

The result is a uniform magnetic field inside the pipe in the fluid region, with a field strength reduced to a fraction α compared with the unperturbed field that would be present for the case when the wall material is non-ferritic. The reduction factor α of the magnetic field is shown in Fig. 8. A reduction of the field strength by orders of magnitude is possible. Magnetic field lines for different permeabilities of the walls are shown in Figs. 9-12. The major result is that the magnetic field inside the duct is strongly reduced but that it is still uniform. This is a special property resulting from the circular shape of the pipe and does not apply to other duct geometries like rectangular ducts.

It is planned to operate different types of test sections with ferritic and non-ferritic materials simultaneously in an experimental campaign in the MEKKA laboratory of the Forschungszentrum Karlsruhe. It is important to notice that the ferritic test section modifies the magnetic field in its neighborhood as can be seen from Fig. 12. For this reason it is necessary to keep other test sections at a save distance of some outer diameters away from the ferritic test section in order to avoid undesired perturbations of the results by the presence of adjacent ferritic channels.

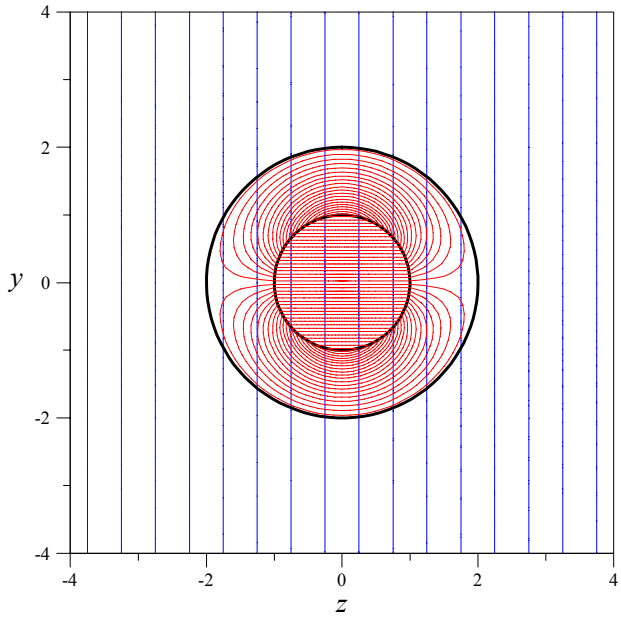

Figure 9: Magnetic field lines (blue) and electric current path (red) through a non-ferritic pipe

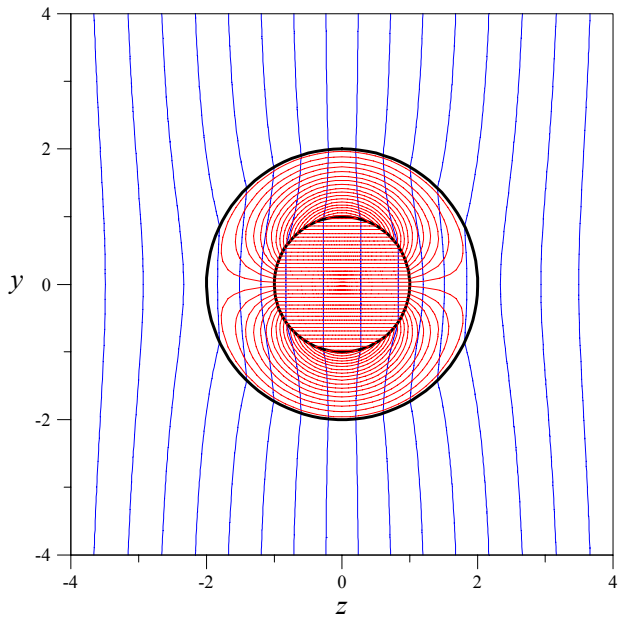

Figure 10: Magnetic field lines (blue) and electric current path (red) through a ferritic pipe with $\mu_w = 2$

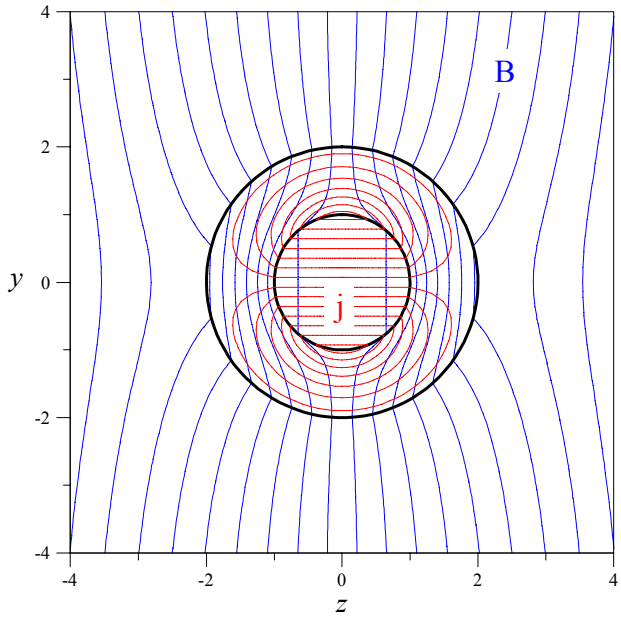

Figure 11: Magnetic field lines (blue) and electric current path (red) through a ferritic pipe with $\mu_w = 10$

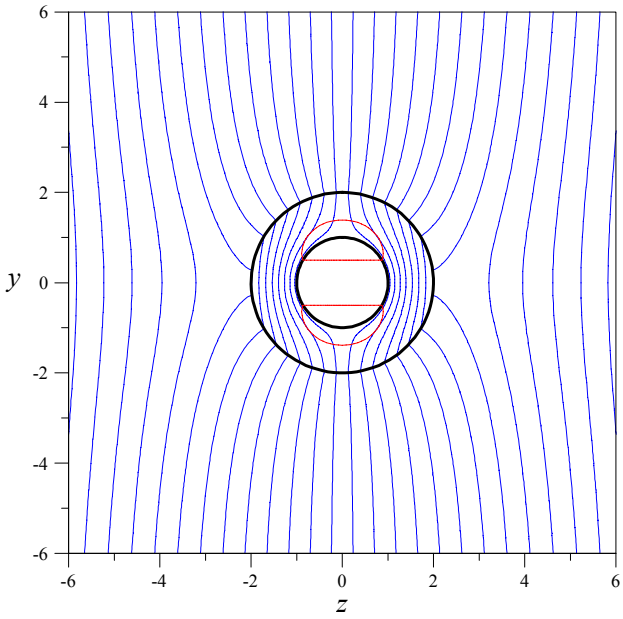

Figure 12: Magnetic field lines (blue) and electric current path (red) through a ferritic pipe with $\mu_w = 100$

We apply now the asymptotic solution procedure as outlined above to flows with the uniform magnetic field transverse through the fluid region. Many results are already known for MHD flows in pipes so that we may use this example to verify the analysis. The uniform field inside the pipe is given by the magnetic potential $A = \alpha z$ so that the general base is determined according to (28) as

$$\mathbf{a}_1 = \hat{\mathbf{x}}, \quad \mathbf{a}_2 = \alpha\hat{\mathbf{y}}, \quad \mathbf{a}_3 = \frac{1}{\alpha}\hat{\mathbf{z}}. \tag{81}$$

The unit vector normal to the duct wall is $\mathbf{n} = \cos\varphi\hat{\mathbf{y}} + \sin\varphi\hat{\mathbf{z}}$. This leads to the interface condition for wall potential according to (60) as

$$\frac{1}{\alpha}\sin\varphi = -\sigma_w \partial_r \Phi_w \quad \text{at } r = 1 \tag{82}$$

for the wall potential determined by the Laplace equation

$$r\partial_r\left(r\partial_r\Phi_w\right) + \partial_{\varphi\varphi}\Phi_w = 0. \tag{83}$$

We express the electric potential in the wall in a Fourier series as

$$\Phi_w = \sum_{i=1}^{\infty} \Phi_{w,i} \sin i\varphi. \tag{84}$$

Due to the condition (82) the exact solution requires only a single Fourier mode. For insulating conditions at the interface to the surrounding atmosphere with $\partial_r\Phi_w = 0$ at $r = R$ we find the solution as

$$\Phi_w = \frac{1}{\alpha\sigma_w}\frac{1}{r}\frac{R^2 + r^2}{R^2 - 1}\sin\varphi \tag{85}$$

in the wall and at the fluid-wall interface at $r = 1$ we have

$$\Phi_w\left(z\right) = \frac{1}{\alpha\sigma_w}\frac{R^2 + 1}{R^2 - 1}\, z\ . \tag{86}$$

We saw that for the present case magnetic field lines are not curved. Since magnetic field lines and isolines of potential coincide we find as solution for the potential in the pipe

$$\Phi\left(y, z\right) = \Phi_w\left(z\right) = \frac{1}{\alpha\sigma_w}\frac{R^2 + 1}{R^2 - 1}\, z \tag{87}$$

The core velocity is determined according to (38) as

$$u = \frac{k}{\alpha^2}\left(1 + \frac{1}{\sigma_w}\frac{R^2 + 1}{R^2 - 1}\right). \tag{88}$$

The core velocity is uniform and a normalization of the flow rate yields the pressure drop as

$$k = \alpha^2\left(1 + \frac{1}{\sigma_w}\frac{R^2 + 1}{R^2 - 1}\right)^{-1}. \tag{89}$$

This result agrees for non-ferritic walls ($\alpha = 1$) with results of Elrod and Fouse (1952). We can compare special limits for which solutions are known. The pressure drop asymptotes for infinitely thick non-ferritic walls with $R \to \infty$, $\alpha = 1$, to the results obtained by Bühler (1998) who finds

$$k = \frac{1}{1 + \frac{1}{\sigma_w}}. \tag{90}$$

The pressure drop in ducts with thin conducting walls where $R = 1 + \varepsilon$ yields for $\varepsilon \ll 1$

$$k = \frac{c}{1+c}\alpha^2. \tag{91}$$

Here, $c = \sigma_w \varepsilon$ is the wall conductance ratio. This result is in accordance with Chang and Lundgren (1961) for $\alpha = 1$. In thin-wall ferritic pipes with $\mu_w \gg 1$ the coefficient α asymptotes to $\alpha \to 2\left(\mu_w \varepsilon\right)^{-1}$. This determines the pressure drop as

$$k = \frac{4}{\left(\mu_w \varepsilon\right)^2} \frac{c}{1+c} \quad \text{for } \varepsilon \ll 1. \tag{92}$$

For ferritic materials the relative permeability is often very large, i.e. $\mu_w \varepsilon > 1$ so that a significant reduction of pressure drop is achieved compared with flows in non-ferritic pipes.

If we consider MHD flows in electrically insulating pipes in which the magnetic field is reduced to a factor α compared to non-ferritic materials, i.e. $B = \alpha \hat{\mathbf{y}}$ we derive from (67) the pressure drop as

$$k = \frac{3\pi}{8Ha}\alpha. \tag{93}$$

All asymptotic results derived above are valid for the case that the magnetic field inside the pipe is still very strong, i.e. $\alpha Ha \gg 1$. For other cases one should use the exact solution for pipe flow (Gold (1962)) which covers the hydrodynamic limit for $\alpha Ha \ll 1$ and replace therein the magnitude of the magnetic field by α.

4.2 Field-dependent magnetic permeability

In the following we consider the regime, when the material reaches its magnetic saturation. We approximate the nonlinear magnetization according to (27) and perform the analysis for the magnetic field as outlined in Sect. 3.1. Results are obtained for ducts with very thick walls, i.e. $R = 5$, which are used during experiments In the MEKKA laboratory of the Forschungszentrum Karlsruhe. The solutions in the ferritic regime have been already outlined before and are not discussed here again. Instead we consider solutions for which the wall material reaches the magnetic saturation. One solution is shown in Fig. 13. Here the externally applied field has a value $B_0 = \frac{1}{2}M_s$. Although the external field is far below the saturation value the magnetic field inside the wall may reach saturation since field lines are concentrated in the wall. This modifies the solution in comparison with the linear ferritic behavior for which we had $B_0 \ll M_s$. The pipe has still good shielding properties but the field penetrating the fluid domain is much higher than for the non-saturated materials. More important, however, is the fact that the magnetic field in the pipe is not uniform as shown in Fig. 14. Moreover, we

observe a significant curvature of field lines. If the external field increases the shielding becomes weaker. The magnetic field inside the pipe increases and approaches the value of the externally applied field as $B_0 \gg M_s$. The magnetic field in the center of the pipe has been measured in the experiment. A comparison of measured and calculated data shows a good agreement. Significant deviations from the linear ferritic regime occur for $B_0 \gtrsim 0.4 M_s$. Then the magnetic field inside the pipe starts to increase strongly before it approaches very slowly the asymptote for non-ferritic materials.

After the magnetic field is known we can determine in a second step the electric potential inside the wall. The solution is efficiently obtained by expanding the wall potential in a Fourier series as $\Phi_w = \sum_{i=1}^{\infty} \Phi_i \sin i\varphi$. In the wall we solve the Laplace equations

$$r\partial_r \left(r\partial_r \Phi_i\right) - i^2 \Phi_i = 0 \tag{94}$$

with boundary conditions at the fluid-wall interface

$$\partial_n \Phi_i = -\frac{1}{\sigma_w}\frac{2}{\pi}\int_o^{\pi} \frac{\partial_n A}{\left(\nabla A\right)^2} \sin i\varphi \, d\varphi \quad \text{at } \Gamma. \tag{95}$$

Remember, the Φ_i are taken in the wall while A is taken in the fluid. After the solution is obtained as

$$\Phi_w = -\sum_{i=1}^{\infty} \frac{\partial_n \Phi_i}{i r^i} \frac{R^{2i} + r^{2i}}{R^{2i} - 1} \sin i\varphi \tag{96}$$

the potential at the interface becomes

$$\Phi_w = -\sum_{i=1}^{\infty} \frac{\partial_n \Phi_i}{i} \frac{R^{2i} + 1}{R^{2i} - 1} \sin i\varphi \quad \text{at } \Gamma. \tag{97}$$

Knowing this result it is possible to construct the relation

$$\Phi\left(A\right) \; = \Phi_w\left(A\right) \quad \text{at } \Gamma \tag{98}$$

which determines uniquely the potential Φ in the fluid for any given value of A inside the pipe. The latter condition ensures that isolines of Φ coincide with magnetic field lines since the potential does not vary along magnetic field lines. The solution of potential in the fluid region is simply obtained by spreading the quantity Φ_w along field lines into the fluid. Isolines of potential in the fluid and in the wall are shown in Fig. 13.

We determine the velocity by similar means. We know that according to (38) the velocity is given by

$$\frac{u}{k} = \frac{1}{\left(\nabla A\right)^2} + \frac{\partial \Phi}{\partial A} \tag{99}$$

and since Φ and A do not vary along field lines we can determine $\partial\Phi/\partial A$ at the wall and spread this quantity along field lines into the fluid. By the flux condition

$$\int_0^1 \int_0^{\pi/2} ur \, d\varphi \, dr = \frac{\pi}{4} \tag{100}$$

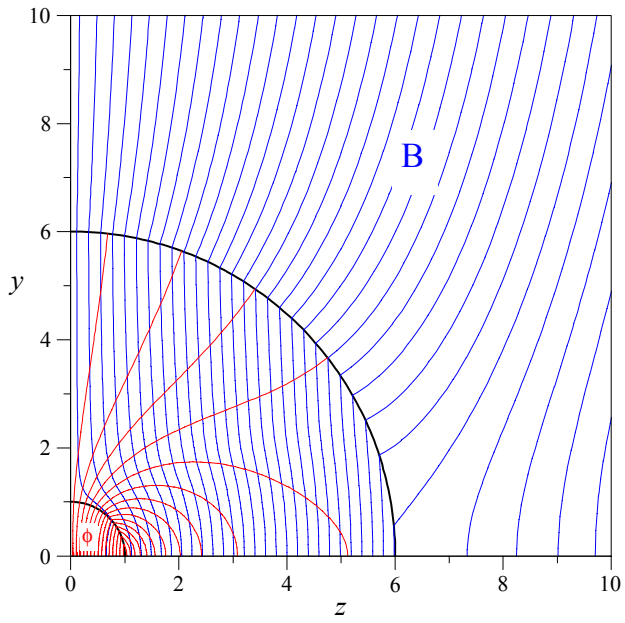

Figure 13: Magnetic field lines (blue) and isolines of electric potential (red) for $B_0/M_s = 0.5$

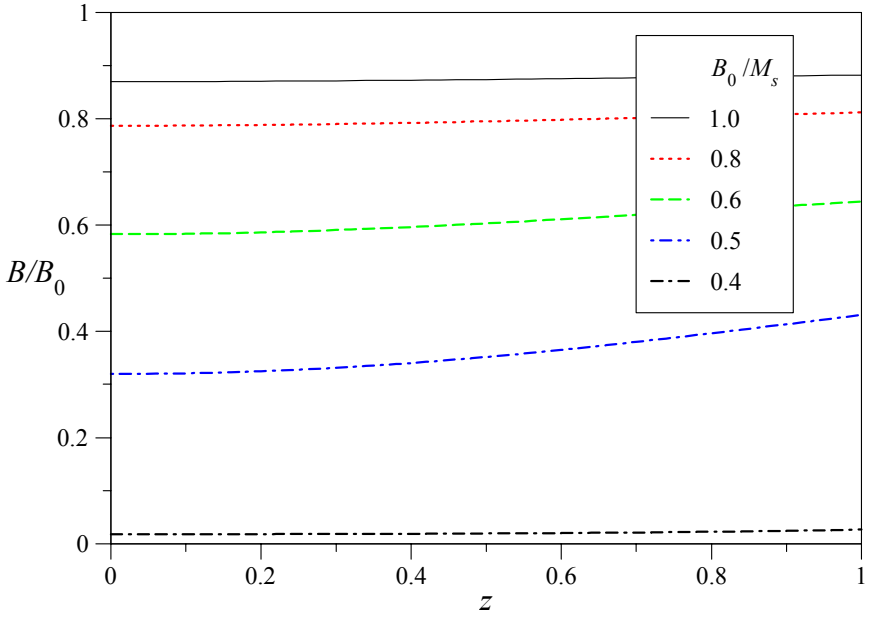

Figure 14: Magnetic field inside the pipe

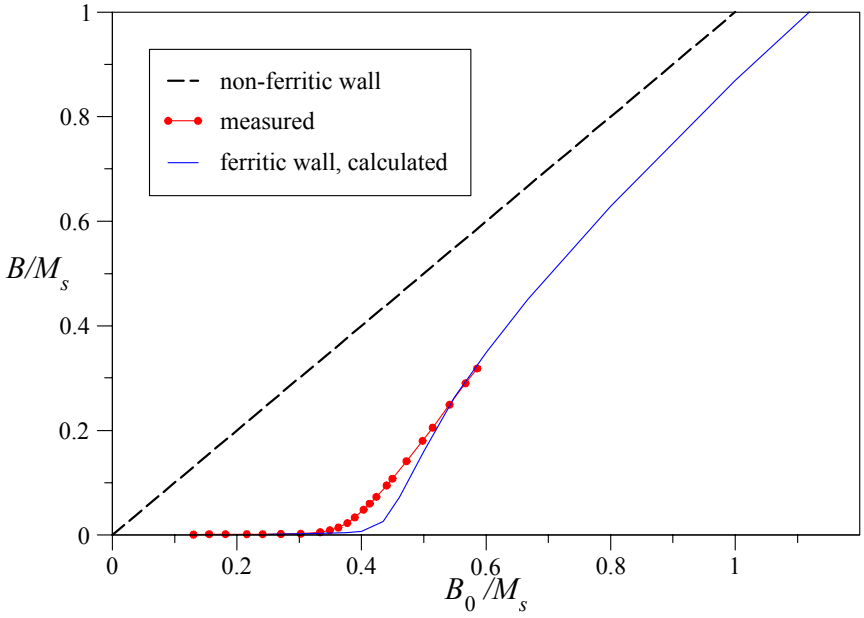

Figure 15: Magnetic field inside a ferromagnetic pipe

we determine the pressure drop k. Results for pressure drop depending on the strength of the applied magnetic field have been calculated. Instead of plotting directly results for pressure drop we assume a relationship similar to (89) as

$$k = \alpha_k^2 \left(1 + \frac{1}{\sigma_w} \frac{R^2+1}{R^2-1}\right)^{-1} \tag{101}$$

and we determine the coefficient

$$\alpha_k = \sqrt{k \left(1 + \frac{1}{\sigma_w} \frac{R^2+1}{R^2-1}\right)} \tag{102}$$

by which the *effective magnetic field* is reduced in comparison with the applied external field. Values of α_k are shown in Fig. 16. The geometry ($R = 5$) and the material data is taken according to the planned experiment in the MEKKA laboratory. The coefficient α which determines the pressure drop exhibits two asymptotes. One is for very strong magnetic fields for which the material reaches perfect saturation everywhere for $B_0/M_s \gg 1$. In this regime we have $\mu_w = \alpha = 1$ and the pressure drop is given by (89) as $k = 0.279$ for $B_0/M_s \to \infty$. For small magnetic fields α would approach very small values according to (78) and the pressure drop would become $k = 9.89 \cdot 10^{-6}$ as $B_0/M_s \ll 1$ for $\mu_w = 700$. We have to notice here, that the magnetic field inside the pipe for the latter case is strongly reduced due to shielding by the ferritic material. On the other hand we assumed high magnetic fields inside the pipe for the asymptotic analysis. The presented results are valid as long as $\alpha Ha \gg 1$. This may not be guarantied in general for small applied fields, even if the Hartmann number is high so that results for $B_0/M_s \ll 1$ are to be considered as academic. For applications related to fusion the magnetic field is

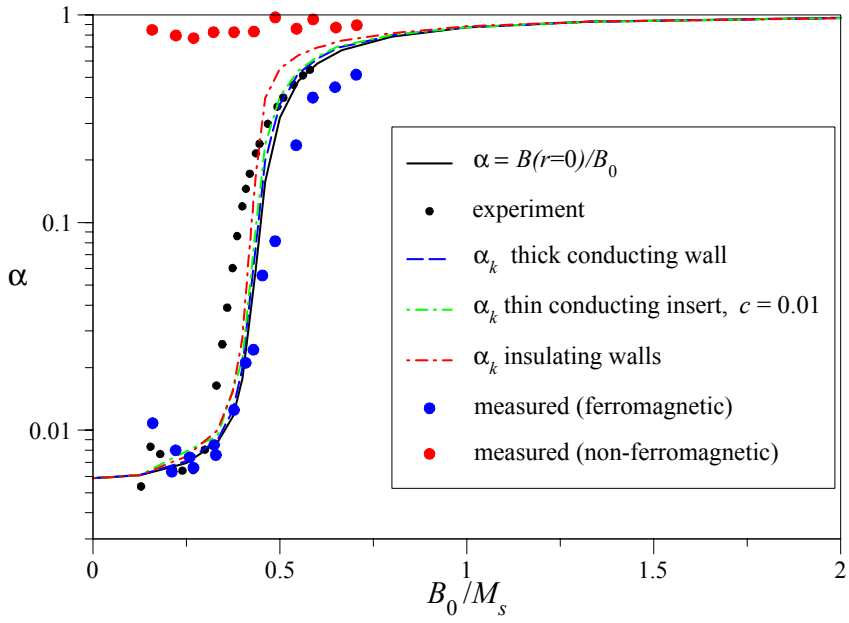

Figure 16: Magnitude of the effective magnetic field inside the pipe responsible for pressure drop depending on the ratio of saturation field M_s and the applied field B_0. The pressure drop for thick conducting walls is obtained according to (101) that for insulated conducting liners by (106) and the pressure drop for perfect electrical insulation of the fluid by (93).

generally very high and the analysis applies perfectly. For a comparison we plot from the data shown in Fig. 14 the value $\alpha\,(r=0) = B\,(r=0)\,/B_0$ evaluated at the center of the duct. Since the magnetic field in the center is the lowest in the pipe it is clear that these values are smaller than those calculated from the pressure drop. Nevertheless, the difference between both results is small. From these considerations we conclude, that if the magnetic field in the center of the pipe is known by either measurements or calculations one can estimate the pressure drop with reasonable accuracy by standard relations.

Isolines of core velocity and velocity profiles along y and z are shown in Figs. 17 and 19. We observe a decrease of the velocity towards the sides as $z \longrightarrow 1$ and an increase of velocity along y. The velocity increase along y can be explained by the fact that due to the curvature of the magnetic field lines the field intensity is lowest near $z = 0$, $y = 1$. For smaller values of the externally applied field, i.e. in the linear ferritic regime the field lines become straight again and the velocity, first along y, but later also along z, becomes more and more uniform and approaches unity. For very strong external fields we observe similar effects, since the relative permeability of the wall asymptotes towards unity so that the field lines are not perturbed by the presence of the wall. Therefore the velocity in the core approaches also unity as $B_0 \gg M_s$.

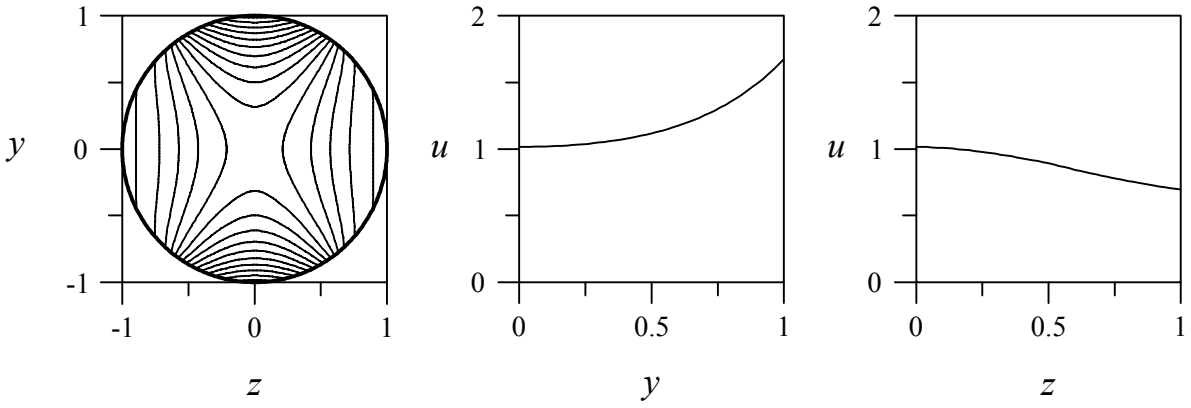

Figure 17: Core velocity for $B_0/M_s = \frac{1}{2}$: Isolines of velocity and velocity profiles along y and z

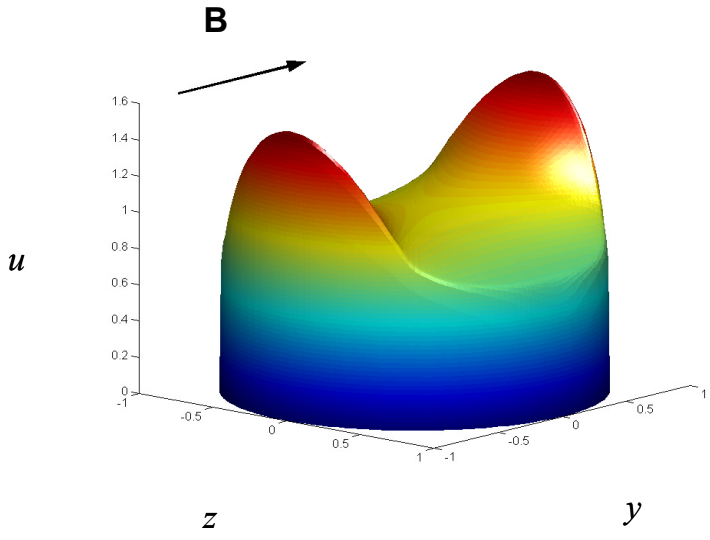

Figure 18: Velocity profile for $B_0/M_s = \frac{1}{2}$

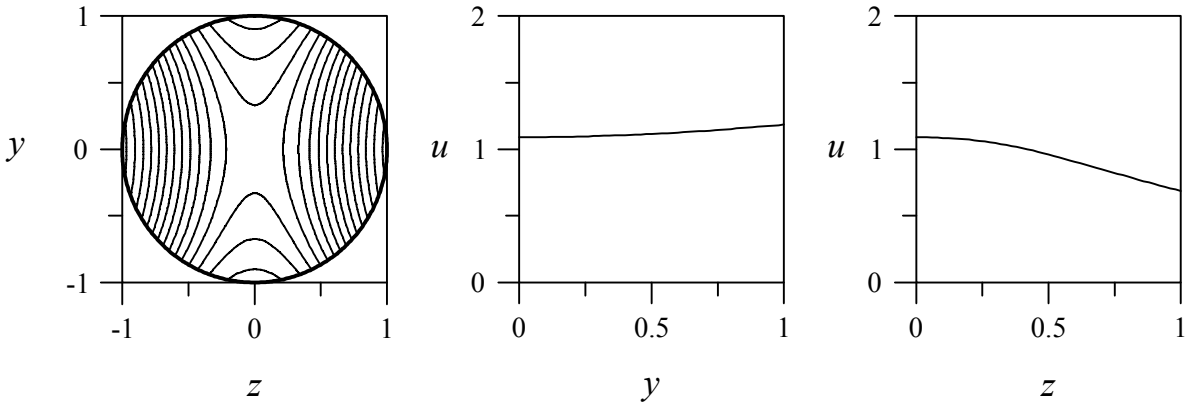

Figure 19: Core velocity for $B_0/M_s = \frac{1}{3}$: Isolines of velocity and velocity profiles along y and z

4.3 Insulated conducting inserts

We have seen that the pressure drop depends essentially on the electrical conductivity of the duct wall. However, for design reasons we have not the freedom to chose wall materials of lower conductivity for reducing the pressure drop. An efficient means could be to cover the fluid-wall interface by an insulating layer in order to prevent currents from entering the well conducting wall. This idea has been proposed e.g. by Malang, Borgstedt, Farum, Natesan and Vitkovski (1995) but it remains to be seen that the insulation material will be able to withstand corrosion by the liquid metal coolant. Even a small number of cracks in the insulation could cancel all benefits. Therefore, a more conservative solution is to protect the insulation by a thin sheet of steel from a direct contact with the fluid. If the steel liner is very thin its electric resistance is large even if the conductivity of the sheet is comparable with that of the fluid. A sketch is shown in Fig. 20.

In the following we assume that the insulating layer is very thin and does not affect the magnetic field. Therefore the analysis presented above applies as well for the determination of the magnetic field. However, since no currents will cross the insulating layer we have to use the boundary condition

$$\partial_n \Phi_w = 0 \tag{103}$$

now at the insulating layer at $R_\phi = 1 + \varepsilon$ while the total major radius of the ferritic wall is still R. We further suppose that the conductivity of the liner is very high compared with the conductivity of the Hartmann layer, i.e. $c = \varepsilon\sigma_w \gg \alpha Ha$. After the magnetic field is obtained the analysis is as outlined before, if we replace in all formulas concerning the potential inside the wall the external radius of the conducting sheet as $R = R_\phi$. For very thin protecting liners with $\varepsilon \ll 1$ the solution for wall potential becomes at leading order

$$\Phi_w = -\sum_{i=1}^{\infty} \frac{\partial_n \Phi_i}{i^2} \sin i\varphi \tag{104}$$

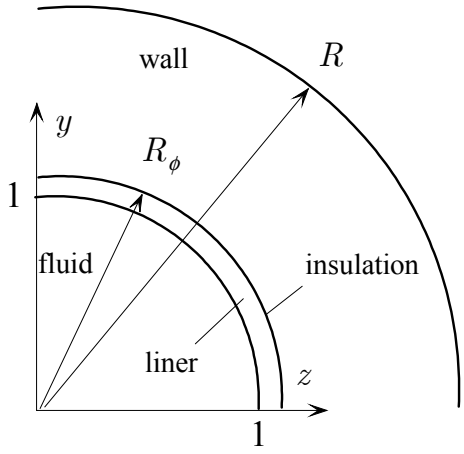

Figure 20: Insulation layer protected from direct contact with the liquid metal by a metallic liner

where

$$\partial_n \Phi_i = -\frac{1}{c}\frac{2}{\pi}\int_o^\pi \frac{\partial_n A}{(\nabla A)^2}\sin i\varphi \, d\varphi. \tag{105}$$

with A taken in the fluid at $r = 1$.

We may also define the coefficient α_k by which the effective magnetic field is reduced in comparison with the externally applied field. For cases with insulating liners we may define the coefficient as $\alpha_k = \sqrt{k\left(1+\frac{1}{c}\right)}$, a quantity that becomes independent if of c as $c \ll 1$. The pressure drop simply evaluates from the latter quantity as

$$k = \alpha_k^2 \frac{c}{1+c}. \tag{106}$$

Results for α_k for flows with insulated liners with $c = 0.01$ are shown in Fig. 16. The results almost agree with those those obtained for thick conducting walls while the pressure drop differs by two orders of magnitude. This result justifies the use of α in order to evaluate pressure drop since the results obtained are more general than the pressure drop itself.

Results for velocity are shown in Fig. 21. Now the isolines of velocity coincide almost with the magnetic field lines. The reason is that for poorly conducting walls the last term in (38) becomes dominant. Since Φ and A do not vary along field lines the velocity is also uniform along magnetic field lines. For both limits as $B_0 \ll M_s$ and as $B_0 \gg M_s$ the magnetic field inside the pipe become uniform and the core velocity asymptotes to unity in the whole cross section.

We supposed above that the conductivity of the liner is high, compared with the conductivity of the Hartmann layers. If the liner becomes very thin, or if there exists a perfectly insulating coating which is in direct contact with the fluid this assumption is no longer justified. For that reason we investigate now the flows for which we may neglect the conductivity of the wall. Such flows arise for $c \ll \alpha Ha$. We calculate the velocity profile according to (66). Normalization of the flow rate yields the pressure

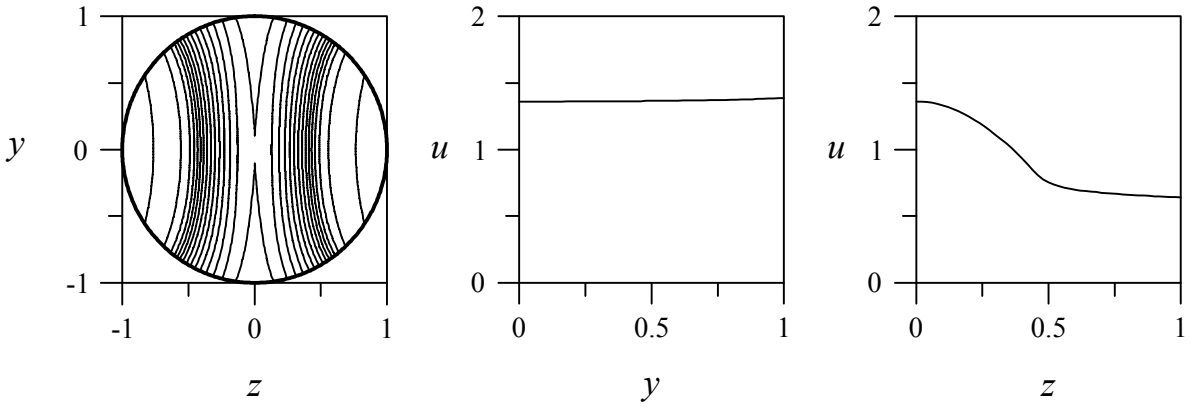

Figure 21: Core velocity for $B_0/M_s = \frac{1}{2}$: Isolines of velocity and velocity profiles along y and z for $c = 0.01$

drop k. The coefficient of effective magnetic field is determined according to $\alpha_k = \frac{8Ha}{3\pi}k$ in order to allow for a comparison with MHD flows in insulating pipes with uniform magnetic fields. Knowing α_k the pressure drop is determined according to

$$k = \frac{3\pi}{8Ha}\alpha_k. \tag{107}$$

Results for α_k are added to Fig. 16. The results indicate that in both liner regimes the value of α_k are close to the value of the magnetic field in the center of the pipe. In an intermediate regime $0.4 < B_0/M_s < 1$, however α_k may be twice as high as $\alpha\,(r = 0)$, reflecting the strong influence of the nonuniformity of the field. Results for velocity are shown in Fig. 22. The isolines of velocity follow the magnetic field lines. The profiles of core velocity show the typical slug flow profile along the field lines. In the other direction we observe similarity with the elliptically shaped profile along z that would be present for uniform magnetic fields as $B_0 \gg M_s$. The latter one has been added to the figure for comparison. Note, the results shown here require for being valid that $\alpha_k Ha \gg 1$.

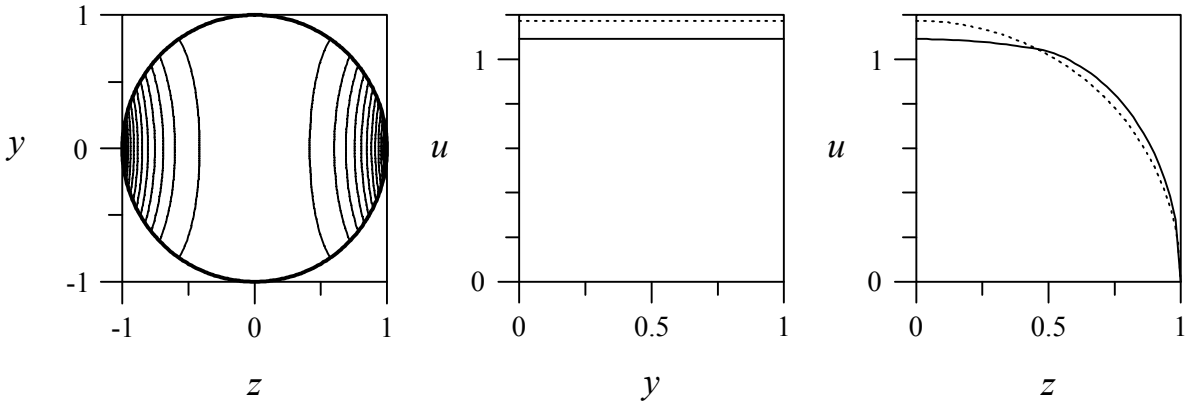

Figure 22: Core velocity for $B_0/M_s = \frac{1}{2}$: Isolines of velocity and velocity profiles along y and z for perfect insulation. The dotted lines are added in order to indicate the solution for uniform magnetic fields, e.g. for $B_0 \gg M_s$

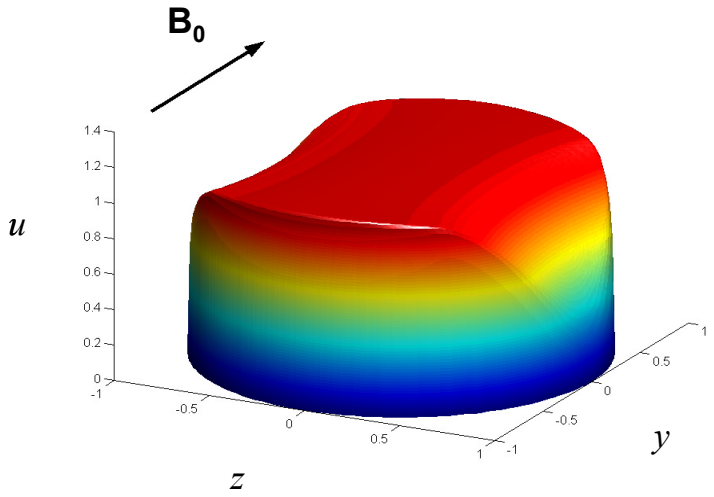

Figure 23: Velocity profiles for $B_0/M_s = \frac{1}{2}$ for perfect insulation.

5 Conclusions

An asymptotic analysis has been performed for the magnetohydrodynamic flow in circular pipes the walls of which are made of ferromagnetic material. The knowledge about pressure drop and flow structure in such pipes, especially with thick walls, is of importance for the European water cooled concept of a fusion blanket. The header of this blanket will be fabricated from ferromagnetic MANET steel which has relative magnetic permeabilities up to $\mu_w = 400$. On the other hand the saturation magnetization is considerably large with $M_s \approx 1.65\,\mathrm{T}$, which is of similar order of magnitude than the externally applied magnetic field $B_0 = 6 - 8\,\mathrm{T}$.

In a first step we determine the magnetic field inside the pipe by introducing a magnetic vector potential. For simplicity we disregard the magnetic hysteresis of the material and assume a uniform permeability of the wall material for $B_0 \ll M_s$. For this case the solution is obtained analytically. The result is that the magnetic field inside the pipe is strongly reduced to a factor $\alpha = B/B_0 \ll 1$ depending on μ_w and the thickness of the wall. On the other hand, the magnetic field remains uniform in the fluid so that we are able to apply all results known from literature in order to predict pressure drop. We should keep in mind that the magnetic fields inside the pipe are very weak and that asymptotic results for MHD flows may become invalid. Then, results covering the hydrodynamic limit should be used to describe the flow more realistically (see e.g. Gold (1962)).

The situation becomes more interesting when the external magnetic field is close to or larger than $B_0 \approx 0.4\ M_s$. For such conditions the material reaches partly magnetic saturation. The result is that the field inside the pipe becomes non-uniform with curved field lines. Again we calculate in a first step the magnetic field in the fluid region. The non-linear equations for magnetic potential in the wall are solved numerically by applying a numerical heat transfer code. The solution outside the wall and inside the pipe is still governed by linear equations and solved analytically. Analytical results obtained for these domains are coupled via the magnetic interface conditions to the numerical procedure during an iterative process. This restricts the computational domain in the numerical calculation to the region of the wall and gives us the possibility to apply an external magnetic field $\mathbf{B}_0 = B_0\hat{\mathbf{y}}$ which is unperturbed by the presence of the ferromagnetic pipe as $r \to \infty$.

After the magnetic field is known we derive by asymptotic techniques, using magnetic coordinates, a solution for the flow in the inviscid core. Viscous boundary layers do not affect the flow in the core if the wall is highly electrically conducting. The currents close their circuit inside the wall and bypass the viscous layer. The viscous layers are purely passive and the solution in the layers simply matches the core velocity smoothly with the no-slip condition at the wall. The solutions for core velocity show a decrease towards the sides as $z \to 1$. The core velocity increases along y and reaches its maximum at $y = 1$, $z = 0$. For stronger magnetic fields the velocity profile in the core becomes gradually flat and approaches unity. It is shown that the pressure drop for a number of

cases can be obtained by a relation as

$$k = \alpha_k^2 \left(1 + \frac{1}{\sigma_w} \frac{R_\phi^2 + 1}{R_\phi^2 - 1} \right)^{-1}, \tag{108}$$

where R_ϕ is the outer radius of the conducting part of the wall. The distinction between R_ϕ and the outer radius of the pipe has been introduced since it is planned to insert in the wall a thin layer of insulating material to decouple electrically the interior region (minor part of the wall and the fluid) from the well conducting thick wall. It is shown that (108) is a very general relation since it applies for very thick conducting walls with $R_\phi = R = 5$ and for very thin liners with $R_\phi = 1 + \varepsilon$ with $\varepsilon \ll 1$. The values of α_k for both cases are practically equal. In the latter case, (108) reduces to

$$k = \alpha_k^2 \left(1 + \frac{1}{c} \right)^{-1}, \tag{109}$$

where $c = \sigma_w \varepsilon$ is the wall conductance ratio.

If the conductivity of the wall becomes much smaller than the conductivity of the Hartmann layers, i.e. for $c \ll (\alpha_k Ha)^{-1}$, the currents close their circuit through the viscous layers. For that case the pressure drop follows a law according to

$$k = \frac{3\pi}{8Ha} \alpha_k \tag{110}$$

and the core velocity shows a profile monotonically decreasing from the maximum value at $z = 0$ to $u = 0$ at $z = 1$.

The strongest dependence of α_k on the externally applied field is observed in a region $0.4\, M_s < B_0 < 2\, M_s$. For stronger magnetic fields α_k approaches unity, $\alpha_k \to 1$ as $B_0 \gg M_s$. If the magnetic field is weaker, α_k approaches the value α obtained by the analytic solution for the linear problem and the pressure drop becomes very small. The pressure drop may eventually reach hydrodynamic values.

References

Alboussière, T., Garandet, J. P. and Moreau, R.: 1996, Asymptotic analysis and symmetry in MHD convection, *Physics of Fluids* **8**(8), 2215–2226.

Bühler, L.: 1995, Magnetohydrodynamic flows in arbitrary geometries in strong, nonuniform magnetic fields. -a numerical code for the design of fusion reactor blankets, *Fusion Technology* **27**, 3–24.

Bühler, L.: 1998, MHD flows in thick-walled ducts, *Technical Report FZKA 6066*, Forschungszentrum Karlsruhe.

Chang, C. and Lundgren, S.: 1961, Duct flow in magnetohydrodynamics, *Zeitschrift für angewandte Mathematik und Physik* **XII**, 100–114.

Elrod, H. G. and Fouse, R. R.: 1952, An investigation of electromagnetic flowmeters, *ASME* **74**, 589–594.

Gold, R. R.: 1962, Magnetohydrodynamic pipe flow. Part 1, *Journal of Fluid Mechanics* **13**, 505–512.

Kulikovskii, A. G.: 1974, Flows of a conducting incompressible liquid in an arbitrary region with a strong magnetic field, *Fluid Dynamics* **8**(1), 462–467. Russian original (1973).

Malang, S., Borgstedt, H. U., Farum, E. H., Natesan, K. and Vitkovski, I. V.: 1995, Development of insulating coatings for liquid metal blankets, *Fusion Engineering and Design* **27**, 570–586.

Müller, U. and Bühler, L.: 2001, *Magnetofluiddynamics in Channels and Containers*, Springer, Wien, New York. ISBN 3-540-41253-0.

Roberts, P. H.: 1967, Singularities of Hartmann layers, *Proceedings of the Royal Society of London* **300**(A), 94–107.

Ruatto, P.: 1996, Entwicklung einer Methode zur Berechnung der elektromagnetischen Kräfte durch Magnetfeldänderungen in ferromagnetischen Strukturen und Anwendung dieser Methode auf den Plasmaabbruch in einem Tokamakreaktor, *Technical Report FZKA 5683*, Forschungszemtrum Karlsruhe.

Shercliff, J. A.: 1953, Steady motion of conducting fluids in pipes under transverse magnetic fields, *Proc.Camb.Phil.Soc.* **49**, 136–144.

Shercliff, J. A.: 1956, The flow of conducting fluids in circular pipes under transverse magnetic fields, *Journal of Fluid Mechanics* **1**, 644–666.

Shercliff, J. A.: 1962, Magnetohydrodynamic pipe flow Part 2. High Hartmann number, *Journal of Fluid Mechanics* **13**, 513–518.